

# MEASUREMENTS OF THE HEAT FLUX, INVERSE BREMSSTRAHLUNG ABSORPTION AND EQUILIBRATION IN AN UNDER-DENSE LASER HEATED PLASMA

A. DYSON, A. E. DANGOR and A. K. L. DYMOKE-BRADSHAW  
Blackett Laboratory, Imperial College, London SW7 3BZ, U.K.

and

R. G. EVANS  
Rutherford Appleton Laboratory, Chilton, Didcot OX11 0QX, U.K.

(Received 25 March 1988)

**Abstract**—A fully ionised hydrogen plasma of initial density  $\approx 5 \times 10^{17} \text{ cm}^{-3}$  and temperature  $\approx 12 \text{ eV}$  is heated using a  $1.053 \mu\text{m}$  laser beam focussed to a spot of  $200 \mu\text{m}$  diameter with an irradiance of  $5 \times 10^{13} \text{ W cm}^{-2}$ . The resulting evolution of the plasma is monitored by Thomson scattering of a second laser beam at  $5265 \text{ \AA}$ . Comparison with a one-dimensional two fluid hydrodynamic simulation shows that the inverse bremsstrahlung absorption coefficient should be modified to include the strong field correction and that the maximum heat flux is about 0.1 of the free streaming limit. The ratio of the electron mean free path to the temperature scale length is about 0.1 and  $T_e/T_i \approx 5$ . The level of ion acoustic turbulence is observed to be small, close to thermal. The ion–electron equilibration rate is found to agree with the usual classical value.

## 1. INTRODUCTION

IT IS well known that theoretical treatments of heat flow based on a first order perturbation theory approach (SPITZER and HARM, 1953) break down for large values of  $\lambda/L$ , where  $\lambda$  is the electron mean free path and  $L$  is the temperature scale length defined by  $\nabla T_e = T_e/L$ . Calculations based on the Fokker–Planck equation (BELL *et al.*, 1981) predict that there is a limit to the maximum heat flux of about 0.1 of the free streaming limit. A maximum heat flux of 0.03 of the free streaming limit was inferred in early experimental work on laser produced plasmas based on measurements of the ion emission, the X-ray emission, or the mass ablation rate (MALONE *et al.*, 1975; YOUNG *et al.*, 1977). However, recent work (KILKENNY *et al.*, 1984) using computer simulations which include thermal transport by fast electrons indicates that the maximum heat flux is about 0.1 of the free streaming limit.

A more direct measurement of the heat flow was reported by GRAY *et al.* (1977) using a  $\text{CO}_2$  laser to heat an under-dense hydrogen plasma. The maximum value for  $\lambda/L$  was 0.3 and the maximum heat flux was found to be limited to 0.03 of the free streaming limit, this low value being attributed to a large level of ion acoustic turbulence. In a similar experiment by WYNDHAM *et al.* (1982) a  $\text{CO}_2$  laser beam of much longer pulse length was used. The maximum heat flux was found to be 0.1 of the free streaming limit at  $\lambda/L$  of 0.07. No turbulence was observed. The definitions for the free streaming limit and the electron mean free path used in this paper follow BELL

*et al.* (1981),  $Q_{fs} = nk_B T_e (k_B T_e / m_e)^{1/2}$  and  $\lambda/L$  such that the Spitzer heat flow for  $Z = 1$  is  $Q_{sp} = 3.2(\lambda/L)Q_{fs}$ .

We report further measurements of the heat flux, using a neodymium laser to heat a small volume of hydrogen plasma. The laser is focussed to give a much larger irradiance of  $5 \times 10^{13} \text{ W cm}^{-2}$  with a pulse length of 1.5 ns, shorter than in the experiments mentioned above. In our experiment Thomson scattered spectra are obtained at two angles to give simultaneous measurements of the electron and ion temperatures and the level of ion acoustic turbulence. The spectra are obtained at four discrete times allowing the plasma evolution to be monitored in a single shot. Comparison with a 1D hydrodynamic code enables the heat flux, inverse Bremsstrahlung absorption and ion–electron equilibration to be determined.

In Section 2 of this paper the experimental details are presented. The results are given in Section 3 and the numerical model is described in Section 4. Comparison between the experiment and the model is discussed in Sections 5 and 6.

## 2. EXPERIMENTAL ARRANGEMENT

The experiment was conducted at the SERC Central Laser Facility using the Vulcan neodymium glass laser. The experimental arrangement is shown in Fig. 1. A slow Z-pinch in hydrogen was used to produce a fully ionised plasma of 30 cm length and about 3 cm diameter. A small volume of the plasma was heated with a  $1.053 \mu\text{m}$  laser beam of 35 J, 1.5 ns fwhm. The beam was focussed transversely into the pinch by a 1 m lens ( $f/10$ ) to a spot of about  $200 \mu\text{m}$  diameter, giving a peak irradiance of  $5 \times 10^{13} \text{ W cm}^{-2}$ . The plasma condition were determined by Thomson scattering of a  $5265 \text{ \AA}$  copropagating probe. The probe consisted of four pulses of 100 ps fwhm separated

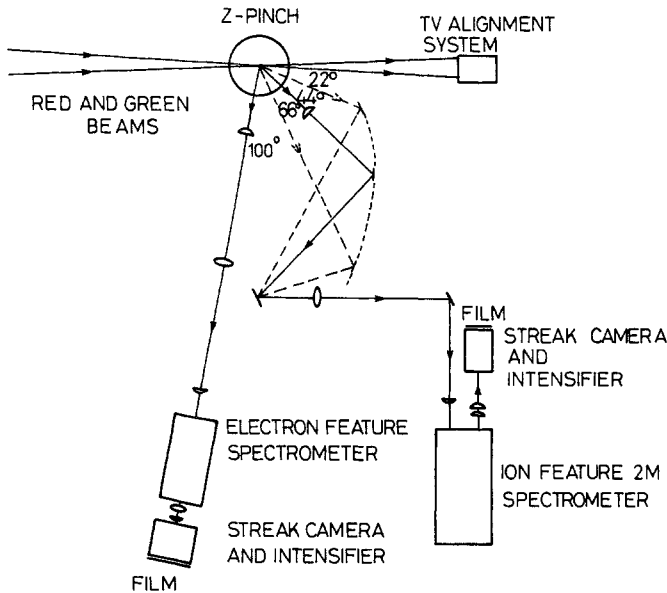


FIG. 1.—Schematic of the experimental arrangement showing the red heating beam, the green probe beams and the two scattering channels.

by 1 ns and focussed by a 1 m lens ( $f/10$ ) with the total energy in the pulses being about 20 J. The relative timing of the Z-pinch plasma, the heating beam and the green probe beams is shown in Fig. 2.

The scattered light from each pulse was monitored in two channels each consisting of a spectrometer and streak camera with the output recorded on HP5 film. The spectrometer slits in both channels were aligned to be in the same plane as the probe beam to maximise the amount of scattered light collected. The scattering volume was a cylinder  $\approx 100 \mu\text{m}$  in diameter and  $\approx 1 \text{ mm}$  long, coaxial with the probe beam. The temporal resolution was determined by the probe pulse duration of about 100 ps. The channel collecting light at 100 degrees had a resolution of  $5 \text{ \AA}$  which was sufficient to resolve the electron feature but not the central ion feature. The spectrally resolved electron feature was used to determine the electron density and temperature. The ion feature was resolved in the second channel which collected light scattered at 22, 44, or 66 degrees with a resolution of  $0.1 \text{ \AA}$ . The resolved ion feature was used to determine the ion temperature and the level of ion acoustic turbulence. This was possible as the amount of stray light was insignificant. The spatial variation of the plasma temperature and density was obtained by moving the focal spot of the heating beam by distances of 0, 200, 400 and  $600 \mu\text{m}$  vertically or horizontally with respect to the fixed scattering volume. This allowed the effect of the heat flux on the velocity distribution to be investigated. For most shots the fill pressure of the Z-pinch was set to give an initial number density of  $2.5 \times 10^{17} \text{ cm}^{-3}$  or  $5 \times 10^{17} \text{ cm}^{-3}$  and a temperature of 8 or 12 eV respectively. Very little variation of the initial density and temperature was observed, indicating the high reproducibility of the pinch. The magnetic field of the pinch was too small to effect the thermal conduction ( $\omega_{ce}\tau_e \ll 1$ ). In the absence of the heating beam the plasma conditions were found to be the same for all the probe pulses indicating that there is little heating by the probe.

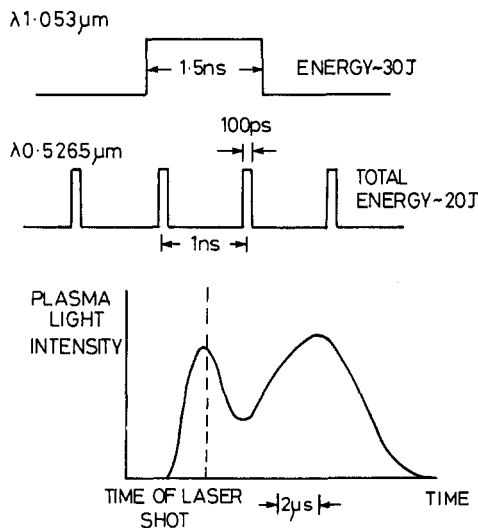


FIG. 2.—Relative timing of the Z-pinch, the heating beam and the four probe pulses.

### 3. EXPERIMENTAL RESULTS

The photographic data of the scattered signals for a typical shot are shown in Fig. 3. The data are digitised using a microdensitometer and then corrected for film response and the spectrometer and streak camera spectral sensitivity. The spectra are then fitted to theoretical Thomson scattering profiles for a thermal plasma (EVANS and KATZENSTEIN, 1969) corrected for instrument response. The electron feature spectra are such that both the electron density and temperature are determined using these quantities as the fitting parameters. The ion temperature is the fitting parameter for the ion feature spectra, using the electron density and temperature obtained from the corresponding electron feature. Full details of the data analysis are to be published elsewhere.

Examples of the fitted spectra are shown in Fig. 4. Extremely good fits are found for the spectra from all four probe pulses, except for the ion feature spectra obtained from the second probe pulse at the focal spot of the heating beam. In these spectra the wings are greater than the expected thermal level indicating the presence of turbulence. This pulse is during the rising edge of the heating beam and here coincides in both time and space with the strongest plasma heating. For these spectra the ion temperature is obtained from the positions of the wings which are shifted by the ion acoustic frequency,

$$\omega_{ac} = k \left[ \frac{\alpha^2}{1 + \alpha^2} \frac{k_B T_e}{m_i} + \frac{3k_B T_i}{m_i} \right]^{1/2} \quad (1)$$

where  $k$  is the differential scattering vector and  $\alpha = 1/(k\lambda_D)$  is the scattering parameter (SHEFFIELD, 1975).

To determine the amount of turbulence the ratio of the integrated ion feature from the second channel to the integrated electron feature is compared with the theoretical ratio assuming a thermal plasma. Good agreement is found except for the spectra obtained from the second probe pulse at the focal spot of the heating beam where the measured ratio is between 1 and 2 times the thermal value. For the scattering at 44 degrees, where most of the data was collected, the integrated ion feature is 1.5 times the thermal level. The measured value of  $T_e/T_i$  is about 5 and at this angle  $k\lambda_D$  is about 0.5. The maximum of the energy spectrum of ion acoustic turbulence is close to this value of  $k\lambda_D$  (DUM *et al.*, 1974). Thus the small enhancement observed indicates that only a low level of turbulence is excited.

The results show that the heating is confined to the focal region of the heating beam with only small temperature increases observed at a distance of 400  $\mu\text{m}$  and none at 600  $\mu\text{m}$ . The measured electron temperatures for an initial density of  $5 \times 10^{17} \text{ cm}^{-3}$  at the focal spot of the heating beam and at 200  $\mu\text{m}$  are shown in Figs. 5 and 6 respectively. The observed heating increases with density as shown in Fig. 7. The measured ion temperatures for an initial density of  $5 \times 10^{17} \text{ cm}^{-3}$  at the focal spot of the heating beam are shown in Fig. 8. The measured plasma conditions show only a slight dependence on irradiance of the heating beam. No change in the density is observed indicating that over the duration of the observations there is no expansion of the heated plasma. The scattered spectra do not show any variation with the direction of displacement from the scattering volume confirming that there is no

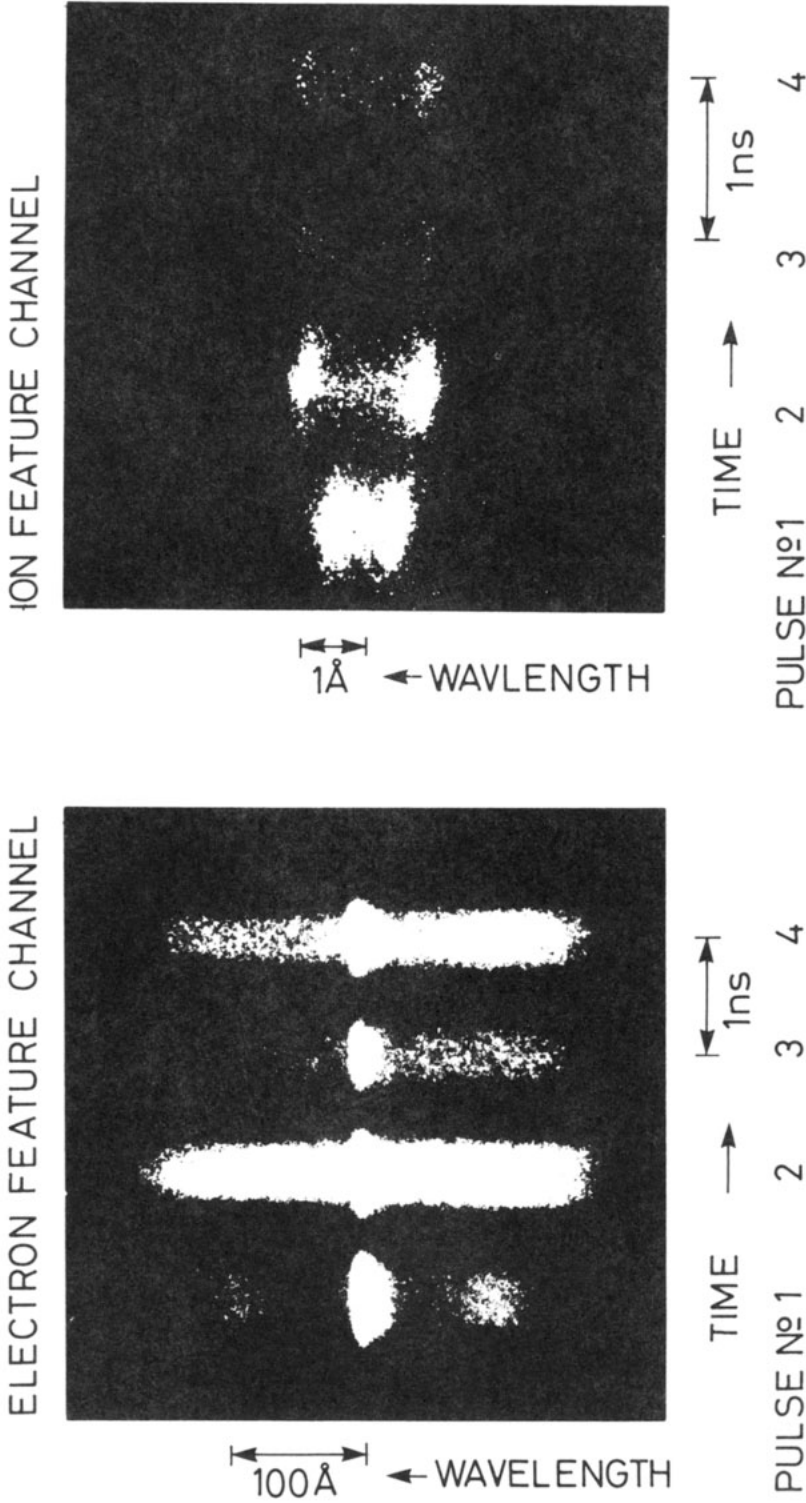


FIG. 3.—Thomson scattering data from a typical shot.

turbulence other than in the focal region. Any skewness in the electron feature due to the heat flow would not be detected. This is because most of the energy is carried by electrons with velocities between 2 and 3 times the thermal velocity and this is outside the range of the measured spectra.

#### 4. MODELLING

The plasma heating is modelled with a 1-D two fluid hydrodynamic simulation based on the MEDUSA code, originally written by CHRISTIANSEN *et al.* (1974). Cylindrical symmetry is assumed and inverse Bremsstrahlung absorption, thermal conduction and ion-electron equilibration are included. The laser is incident along the axis and has a Gaussian radial intensity profile with width equal to the measured spot size. The model assumes that the plasma is fully ionised with the initial plasma conditions set to the experimentally measured values.

The classical inverse Bremsstrahlung absorption cross-section is modified by the strong field correction (PERT, 1972; RAND, 1964) to allow for the reduction in collision frequency when the electron oscillating velocity in the light wave,

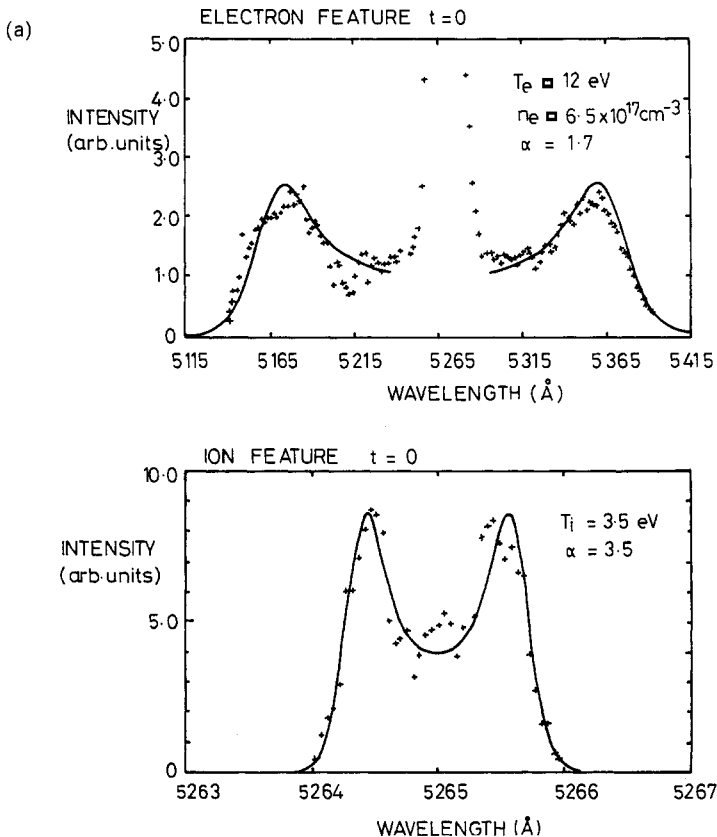


FIG. 4.—Typical scattering profiles with the computer generated best fit. The ion feature spectrum for the second probe pulse at  $t = 1 \text{ ns}$  indicates turbulence.

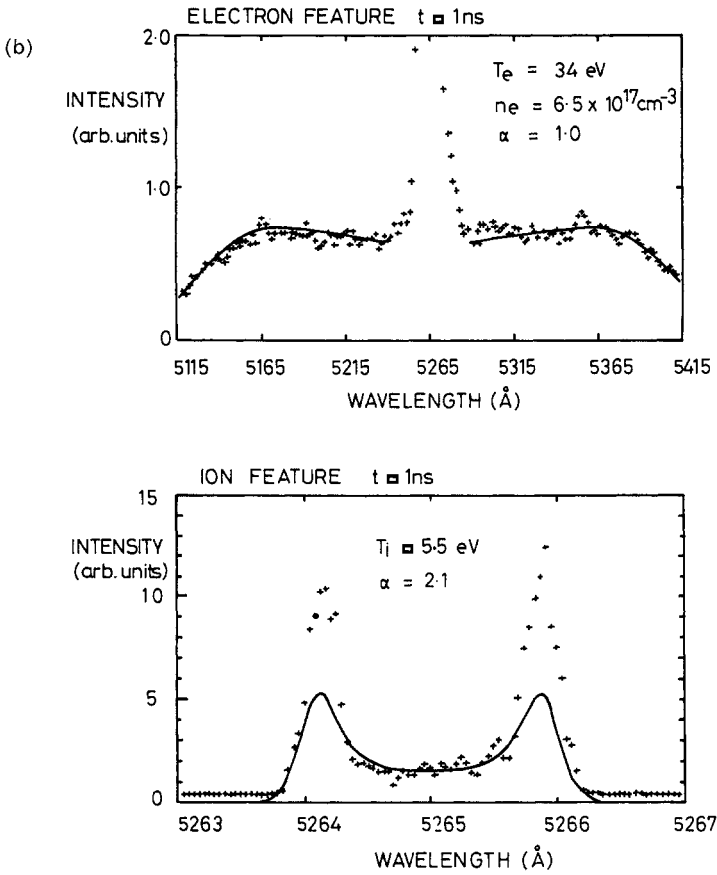


FIG. 4.—continued

$v_{\text{osc}} = eE/m_e\omega$ , exceeds the thermal speed,  $v_e = (k_B T_e/m_e)^{1/2}$ . The effective collision frequency is taken to be

$$v_{\text{eff}} = v_{ei} \frac{v_e^3}{[v_{\text{osc}}^2 + v_e^2]^{3/2}}. \tag{2}$$

Here  $v_{ei}$  is the classical electron-ion collision frequency in which the Coulomb logarithm  $\ln \Lambda = \ln(r_{\text{max}}/r_{\text{min}})$  has  $r_{\text{max}} = v_e/\omega$ , where  $\omega$  is the heating beam laser frequency, and  $r_{\text{min}}$  is the minimum of  $e^2/4\pi\epsilon_0 k_B T_e$  and  $\hbar/(m_e k_B T_e)^{1/2}$ .

The heat flux is restricted to the electron free streaming limit by taking it to be sharply limited by

$$Q = \min(Q_{\text{sp}}, fQ_{\text{fs}}) \tag{3}$$

or harmonically limited by

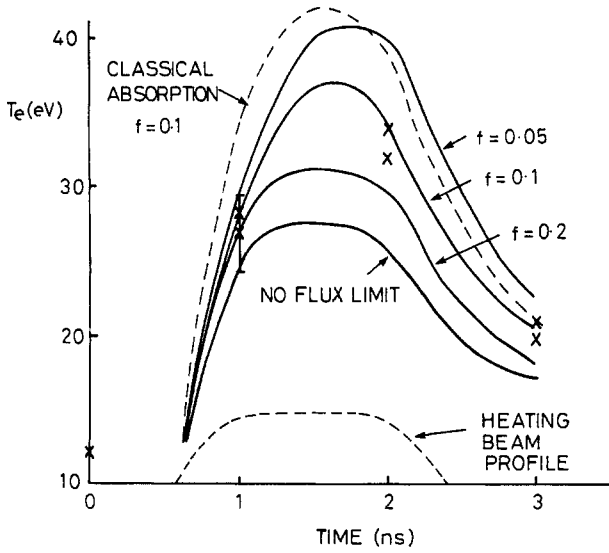


FIG. 5.—Measured electron temperatures at the focal spot of the heating beam for an electron density of  $5 \times 10^{17} \text{ cm}^{-3}$ . The solid lines show the predicted temperatures with strong field corrected absorption for various values of the flux limit  $f$ .

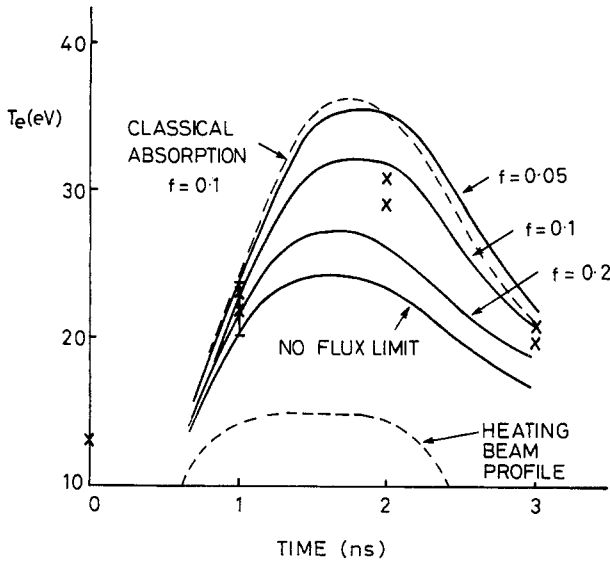


FIG. 6.—Measured electron temperatures at  $200 \mu\text{m}$  from the focal spot of the heating beam for an electron density of  $5 \times 10^{17} \text{ cm}^{-3}$ .

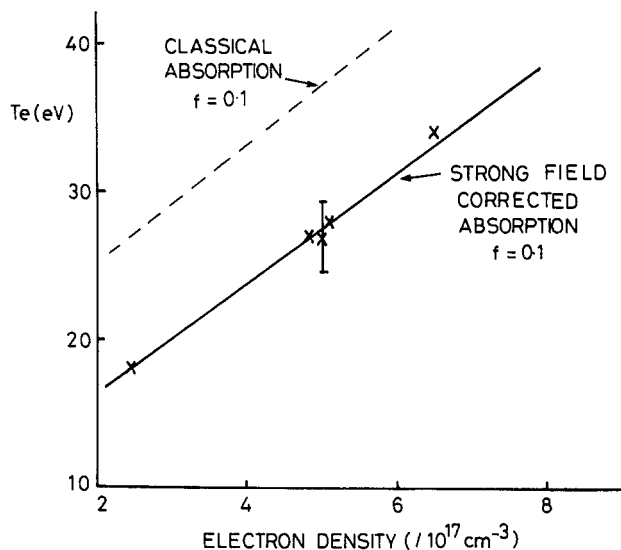


FIG. 7.—Measured electron temperatures at the focal spot of the heating beam for various electron densities. The solid line shows the predicted temperatures for strong field corrected absorption and the broken line for classical absorption, with the flux limit  $f = 0.1$ .

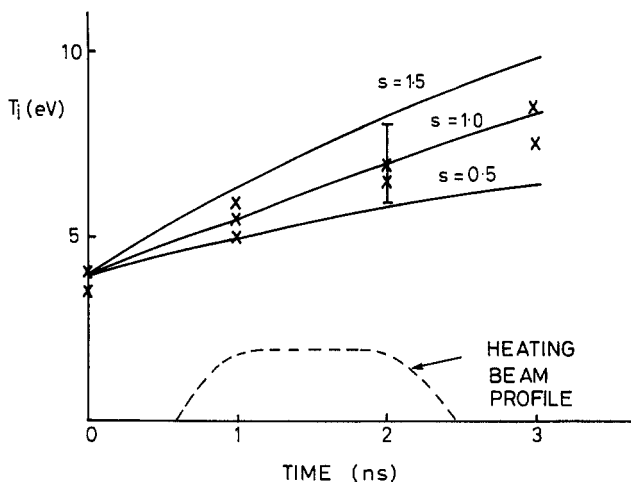


FIG. 8.—Measured ion temperatures at the focal spot of the heating beam for an electron density of  $5 \times 10^{17} \text{ cm}^{-3}$ . The solid lines show the predicted temperatures for different values of the equilibration multiplier  $s$ .

$$\frac{1}{Q} = \frac{1}{Q_{\text{sp}}} + \frac{1}{fQ_{\text{fs}}}. \quad (4)$$

Here  $Q_{\text{sp}}$  is the Spitzer heat flow

$$Q_{\text{sp}} = 3.2(\lambda/L)nk_B T_e (k_B T_e/m_e)^{1/2} \quad (5)$$

and  $Q_{\text{fs}}$  is the free streaming limit, defined by

$$Q_{\text{fs}} = nk_B T_e (k_B T_e/m_e)^{1/2} \quad (6)$$

where the flux limit  $f$  is an adjustable constant. The ratio of the electron mean free path  $\lambda$  to the temperature scale length  $L = T_e/\nabla T_e$  is

$$\lambda/L = 1.44 \cdot 10^{13} T_e \text{ (eV)} |\nabla T_e \text{ (eV cm}^{-1})|/n \text{ (cm}^{-3}) \ln \Lambda \quad (7)$$

where the Coulomb logarithm is given by the usual expression.

The ion–electron equilibration rate is taken to be a multiple of the classical expression so that the effective equilibrium rate is

$$v_{\text{eff}}^e = s v_{ei}^e \quad (8)$$

where

$$v_{ei}^e = 3.2 \cdot 10^{-9} n \text{ (cm}^{-3}) \ln \Lambda / T_e \text{ (eV)}^{3/2} \text{ s}^{-1} \quad (9)$$

and the equilibration multiplier  $s$  is an adjustable constant.

## 5. COMPARISON WITH EXPERIMENT

Figures 5–8 show how the calculated temperatures depend on the flux limit  $f$ , classical and strong field corrected absorption and the equilibration multiplier  $s$ .

The temperatures predicted at the time of the second probe pulse, about 400 ps after the start of the heating beam, are only slightly dependent on the flux limit  $f$ . This can be seen in Figs. 5 and 6 where with classical absorption too much heating results but with strong field corrected absorption good agreement is obtained. At the peak of the heating beam the strong field correction reduces the absorption coefficient by more than 50%. This is further illustrated in Fig. 7 which shows that the predicted temperatures with strong field corrected absorption are in agreement with the measured temperatures for various densities.

The temperatures predicted at the time of the third probe pulse, close to the end of the heating beam, and at the time of the fourth probe pulse, about 1 ns after the heating beam, depend on the value of the flux limit. Figures 5 and 6 indicate that the results are consistent with  $f = 0.12 \pm 0.05$  in the case of harmonically limited heat flow [equation (4)]. For sharply limited heat flow [equation (3)] it is found that  $f = 0.09 \pm 0.02$ . The maximum value for  $\lambda/L$ , determined from the spatial profiles of the predicted electron temperature, is about 0.1. Thus, if no heat flux is imposed the

Spitzer heat flow would give a maximum heat flux of about 0.3 of the free streaming limit [equation (5)]. The simulations show that if the classical absorption coefficient is used with the Spitzer heat flow then there is too little heating at the focal spot and too much heating outside.

Figure 8 shows that the measured ion temperatures are best modelled by the classical electron-ion equilibration rate to within 50%. The predicted ion temperatures are only slightly dependent on the value chosen for the flux limit. The increase in ion temperature is small, consistent with the equilibration time being very much longer than the duration of the heating beam.

The predicted decrease in electron density due to hydrodynamic expansion is small in agreement with the observation of no measurable change in density. It is found that changing the laser irradiance by 50% results in changes in the predicted temperatures of about 1 eV. This is as a result of the saturation of the inverse Bremsstrahlung absorption due to the strong field correction.

## 6. DISCUSSION AND CONCLUSIONS

The maximum heat flux is observed to be limited to about 0.1 of the free streaming limit. Temperature gradients with  $\lambda/L$  of about 0.1 are generated and  $T_e/T_i$  is about 5. Only a very low level of ion acoustic turbulence is observed. The strong field correction should be included in the inverse Bremsstrahlung absorption coefficient when the laser irradiance is large. The ion-electron equilibration rate is found to be within 50% of the classical value.

Our simulation code for the experimental conditions of GRAY *et al.* (1980) gives a poor fit to the quoted measured temperatures for all values of the flux limit. The best fit is for a flux limit of  $f = 0.06$  with  $\lambda/L = 0.2$  and should be compared with the published values of  $f = 0.03$  and  $\lambda/L = 0.3$ . The low value of the flux limit was attributed to ion acoustic turbulence. A surprisingly large value of  $\delta n/n = 0.09$  was inferred from a 10 times observed enhancement of the unresolved scattered signal close to the incident probe frequency at  $k\lambda_D = 2$ . The ion acoustic energy spectrum is proportional to  $k^4 S_{io}(k)$ , where  $S_{io}(k)$  is the integrated ion feature (GRAY *et al.*, 1980). Using this and the ion acoustic energy spectrum of DUM *et al.* (1979) it can be shown that the observed 10 times enhancement corresponds to a greater than 150 times enhancement at  $k\lambda_D = 0.5$ , close to where the energy spectrum peaks. This should be compared with the 1.5 times enhancement observed in our experiment at  $k\lambda_D = 0.5$ . A higher level of turbulence in the experiment of GRAY *et al.* (1980) may possibly be due to the electron mean free path being comparable to the focal spot size. This results in a large return current of electrons giving rise to ion acoustic turbulence. In our experiment the mean free path was only about 0.15 of the focal spot size.

The simulation is in good agreement with the results of WYNDHAM *et al.* (1982) for a maximum heat flux of 0.1 of the free streaming limit with  $\lambda/L = 0.07$ . This result and our value for the flux limit agree with calculations based on the Fokker-Planck equation (BELL *et al.*, 1981) which limit the maximum heat flux to about 0.1 of the free streaming limit.

*Acknowledgements*—We particularly wish to thank M. LEWIS for her considerable contribution to the experiment. We would also like to thank A. COLE and W. TONER for their participation and interest.

## REFERENCES

- BELL A. R., EVANS R. G. and NICHOLAS D. J. (1981) *Phys. Rev. Lett.* **46**, 247.  
CHRISTIANSEN J. P., ASHBY D. and ROBERTS K. V. (1974) *Comput. Phys. Commun.* **7**, 271.  
DUM C. T., CHODURA R. and BISKAMP D. (1974) *Phys. Rev. Lett.* **32**, 1231.  
EVANS D. E. and KATZENSTEIN J. (1969) *Rep. Prog. Phys.* **32**, 207.  
GRAY D. R., KILKENNY J. D., WHITE M. S., BLYTHE P. and HULL D. (1977) *Phys. Rev. Lett.* **39**, 1270.  
GRAY D. R. and KILKENNY J. D. (1980) *Plasma Physics* **22**, 81.  
KILKENNY J. D. *et al.* (1984) *Phys. Rev. Lett.* **53**, 2563.  
MALONE R. C. *et al.* (1975) *Phys. Rev. Lett.* **34**, 721.  
PERT G. J. (1972) *J. Phys. A*, **5**, 506.  
RAND S. (1964) *Phys. Rev.* **136B**, 231.  
SHEFFIELD J. (1975) *Plasma Scattering of Electromagnetic Radiation*. Academic Press, New York.  
SPITZER L. and HARM R. (1953) *Phys. Rev.* **89**, 977.  
WYNDHAM E. S., KILKENNY J. D., CHUAQUI H. H. and DYMOKE-BRADSHAW A. K. L. (1982) *J. Phys. D* **15**, 1683.  
YOUNG F. C. *et al.* (1977) *Appl. Phys. Lett.* **30**, 45.